Bond Graph Modeling of Muscle-Tendon Actuation of a Phalange

Sandeep Kumar UPPAL*, Anand VAZ

*Department of Mechanical Engineering, Dr. B. R. Ambedkar National Institute
of Technology, Jalandhar, Punjab, India; e-mail: anandvaz@ieee.org*
* Corresponding Author e-mail: skuppal@rediffmail.com

In musculoskeletal actuation systems, it is essential to understand and analyze the extension and force patterns generated in the muscle-tendon units (MTUs) responsible for the motion of a phalange. This work proposes a systematically developed bond graph model for the muscle-tendon actuation system for the desired motion of the phalange of the hand. The phalange is represented by a cylindrical rigid body, actuated by four MTUs attached to it symmetrically. The MTU is based on Hill's muscle model. The role of the central nervous system (CNS) that commands desired motions to the phalange is emulated through a virtual domain in the model. The virtual domain decides the activation pattern of MTUs. Accordingly, the MTUs apply forces on the phalange to achieve the desired motion. Simulation results for important motions such as flexion-extension, adduction-abduction, and circumduction show that the model effectively captures the dynamics of the musculoskeletal actuation system.

Keywords: musculoskeletal actuation, bond graph, muscle-tendon units, central nervous system, simulation.

NOTATION

C_v, C_r	–	center of the mass of the virtual and real phalange,
$I : \left[{}_{C_v}^{0} I_v \right]$, $\left[{}_{C_r}^{0} I_r \right]$	–	inertia tensor of the virtual and real phalange, respectively, with respect to the center of mass of the body and expressed in inertial frame $\{0\}$, $\in \mathbb{R}^{3 \times 3}$,
M_v, M_r	–	mass of the virtual and real phalange,
$[M_v]$, $[M_r]$	–	translational inertial element of the virtual and real phalange, $\in \mathbb{R}^{3 \times 3}$,
${}_{C_v}^{0}\overline{p}_v$, ${}_{C_r}^{0}\overline{p}_r$	–	angular momentum of the virtual and real phalange, with regard to the center of phalange mass and expressed in inertial frame $\{0\}$, $\in \mathbb{R}^{3 \times 1}$,
${}^{0}\overline{p}_v$, ${}^{0}\overline{p}_r$	–	linear momentum of the virtual and real phalange expressed in inertial frame $\{0\}$, $\in \mathbb{R}^{3 \times 1}$,
${}_{0}^{0}\overline{\omega}_v$, ${}_{0}^{0}\overline{\omega}_r$	–	angular velocity of the virtual and real phalange, respectively, observed and expressed in inertial frame $\{0\}$, $\in \mathbb{R}^{3 \times 1}$,

${}_0^0\dot{\bar{r}}_{Cv}$, ${}_0^0\dot{\bar{r}}_{Cr}$	–	translational velocity of the virtual and real phalange, respectively, observed and expressed in inertial frame $\{\boldsymbol{0}\}$, $\in \mathbb{R}^{3\times 1}$,
${}_{C_v}^{0}\bar{r}_{O_{11v}}$, ${}_{C_r}^{0}\bar{r}_{O_{11}}$	–	position vector of point O_{11v}, O_{11} on the virtual and real phalange, respectively, with regard to their center of mass and expressed in inertial frame $\{\boldsymbol{0}\}$, $\in \mathbb{R}^{3\times 1}$,
${}_{C_v}^{0}\bar{r}_{O_{12v}}$, ${}_{C_r}^{0}\bar{r}_{O_{12}}$	–	position vector of point O_{12v}, O_{12} on the virtual and real phalange with regard to their center of mass, respectively, and expressed in inertial frame $\{\boldsymbol{0}\}$, $\in \mathbb{R}^{3\times 1}$,
${}_{C_v}^{0}\bar{r}_{Pv}$, ${}_{C_r}^{0}\bar{r}_{P}$	–	position vector of tendon insertion point on the virtual and real phalange with regard to their center of mass respectively and expressed in inertial frame $\{\boldsymbol{0}\}$, $\in \mathbb{R}^{3\times 1}$,
${}_0^0\dot{\bar{r}}_{Pv}$, ${}_0^0\dot{\bar{r}}_{P}$	–	translational velocity of the tendon insertion location on the virtual and real phalange, respectively, observed and expressed in inertial frame $\{\boldsymbol{0}\}$, $\in \mathbb{R}^{3\times 1}$,
$[{}_{1v}^{0}R]$, $[{}_{1}^{0}R]$	–	rotation matrix describing the orientation of virtual frame $\{\boldsymbol{1_v}\}$ and real phalange $\{\boldsymbol{1}\}$ with respect to inertial frame $\{\boldsymbol{0}\}$, $\in \mathbb{R}^{3\times 3}$,
$C:[K_t]$, $C:[K_r]$	–	stiffness element matrix at translational and rotational coupling, $\in \mathbb{R}^{3\times 3}$,
$R:[R_t]$, $R:[R_r]$	–	damping element at translational and rotational coupling, respectively, $\in \mathbb{R}^{3\times 3}$,
$C:[K_{SE}]$, $C:[K_{PE}]$	–	stiffness element for series-elastic element and parallel elastic element in the Hill's muscle model respectively, $\in \mathbb{R}^{1\times 1}$,
$R:R_{DE}$	–	damping element in Hill's muscle model, $\in \mathbb{R}^{1\times 1}$,
$S_E:T_{CE}$	–	force from a contractile element in Hill's muscle model, $\in \mathbb{R}^{1\times 1}$,
$S_E:F_{PT}$	–	pre-tension force,
COM	–	center of mass.

1. Introduction

Most of the tasks that we all perform daily such as grasping, manipulating objects, playing music, writing, etc., require the interaction of the hands with the environment [1]. All these interactions require specific actuation forces and moments to be applied by the various muscle-tendon units of the human hand [2]. All these actions seem to be very simple in nature, but a detailed computation of muscle-tendon actuation forces is performed at the backend by the central nervous system (CNS). Muscle tendons play an essential role in generating forces and transferring the forces to the bone to control the posture and joint motion of the skeletal system. The fingers of the hand can reach the desired position accurately only if necessary actuation is provided by the involved muscle-tendon units. Determination of the pattern of extensions and forces required for a task motion is quite a significant aspect of the muscle-tendon structure. Capturing the mechanics of the muscle-tendon units for the actuation mechanism of the phalange (rigid bone) motion is of significant interest in understanding the behavior of musculoskeletal actuation.

The muscle tendons possess high mechanical strength and a complex nonlinear viscoelastic characteristic dependent on the mechanical strain rate [3]. The muscle tendons become stiffer at a high strain rate, increasing the capability to transmit higher muscular loads [2]. The magnitude of the force and the corresponding torque developed at the joints significantly depend on the number of muscle tendons connected to the phalange, the tendon insertion location on the phalange, the origin of the muscle, and the amount of pre-tension. The intricate location and orientation of the joint motion axes increase the complexity of the system. Various motions such as flexion-extension, abduction-adduction, opposition, and circumduction are achieved through the coordinated actuation of the muscle tendons.

It is challenging to understand the dynamic behavior of each muscle-tendon unit for the desired motion through in-vivo and in-vitro studies. It is difficult to interpret the muscle forces and the simultaneous contribution of each electromyogram (EMG) signal using in-vivo studies [4]. Also, there can be considerable variation in EMG patterns from trial to trial and it is difficult to obtain information on the excitation of deep muscles using the in-vivo analysis. On the other hand, it is difficult to obtain the complete detail of responses from the muscle tendons during joint motion using in-vitro analysis, as the tissues are not alive in cadaver specimens. To gain insight into the mechanics of muscle-tendon actuation, it is necessary to develop a computational model for the system.

This work presents a bond graph-based computational model to actuate the joint motion of a phalange through muscle-tendon actuation. To obtain the motion of the phalange to follow desired trajectory profiles, the actuation of the associated muscle-tendon units is required. The input for the actuation is taken from a commanded virtual phalange considered to emulate the role of the CNS. The combined system of virtual and real phalange has been developed to understand the dynamic behavior of the system. MTUs themselves determine the necessary extension patterns and the forces that need to be applied at the respective insertion points of the tendons on the real phalange taking inputs through virtual muscle-tendon controllers (MTC). Some pre-tension always exists in the muscle-tendon units for supporting a posture, even in a steady state. The authors have also incorporated the pre-tension in the muscle-tendon structure to avoid slackening. It maintains the muscle tendons in a taut condition. This proposed model will help to gain knowledge on the behavior of the muscle-tendon structure under dynamic conditions. The system will be able to determine the pattern of muscle-tendon extensions required and the actuation forces generated in each muscle-tendon unit for the desired kind of motion imposed on the system.

Studies based on steady-state postures have been carried out by various researchers. In 1985, An *et al.* [5] studied the force analysis of the index finger for the tip pinch, and pulp pinch task. Similar work on the thumb was performed by

Johanson *et al.* [6] for key pinch and opposition pinch. Sancho-Bru *et al.* [7] developed a 3D model of the human finger for estimating the muscular forces during finger movements by minimizing the stress function. A musculoskeletal model of a lumped-parameter human leg has been proposed by Wojcik using a bond graph [8]. A general mathematical model for kinematics analysis of the hand was developed by Chen Chen *et al.* [9]. The actuation mechanism of the musculoskeletal joint was modeled for flexion-extension of the bone by Vaz *et al.* [10]. Later on, the extensor mechanism of the finger based on Winslow's rhombus tendinous network was developed by Vaz *et al.* [11]. Mishra and Vaz [12] analyzed the actuation of the finger using tendon control as a string-tube mechanism for the active and passive systems using a bond graph. The CNS plays a very significant role in controlling the dynamics of the various motions of the hand [13]. Mishra and Vaz [14] proposed a model for controlling the active finger through the virtual domain as a part of the CNS.

A lot of research has been conducted on musculoskeletal behavior, but mostly on certain static postures. Very little has been done so far in predicting and analyzing the extensions and force patterns generated by the muscle-tendon structure for performing a task considering dynamics. Analyzing the dynamic behavior of the muscle-tendon structure is a challenging task. To understand the dynamics of joint actuation through the muscle tendons, certain issues need to be addressed namely the number of muscle tendons involved, the coordinated patterns of extensions among the associated muscle tendons, the force patterns to be applied taking into account the nonlinear force – strain characteristics, and the pre-tension. All these issues are also required to be explored from the control point of view through CNS and have been addressed in this work.

To this end, Sec. 2 elaborates on the structure of the proposed musculoskeletal model of a phalange with muscle-tendon actuation for a generalized three-dimensional system. The control scheme for emulating the role of the CNS using the concept of virtual phalange and virtual MTC, and the nonlinear mechanics of the muscle-tendon model are also explained. The dynamics of the entire system is modeled using the graphical approach of the multibond graph in Sec. 3. The construction of the multibond graph model and the derivation of system equations from it are also explained. The proposed multibond graph model is simulated for flexion-extension, adduction-abduction, and circumduction motions. Simulation results showing the dynamic behavior are analyzed in Sec. 4. Concluding remarks are discussed in Sec. 5.

2. Modeling the musculoskeletal actuation system

A human hand consists of 14 phalanges and 5 metacarpal bones [15]. The musculoskeletal actuation system of the phalange consists of a complex mus-

culoskeletal network of MTUs. Various extrinsic and intrinsic muscles are connected to the phalanges at different insertion locations on the phalange. The MTUs generate different forces under different stimuli and provide moments at the joints for the motion.

The important questions that arise are as follows. For the phalange to have desired motion, what would be the extension and force patterns required to be generated by individual muscle tendons that actuate it? The pre-tension as well as the nonlinear force – strain characteristics of the MTUs are also required to be taken into account. How could the actuation efforts required to be generated by the CNS for the performance of desired tasks be determined?

The prime objective of this research is to study the dynamic behavior of the muscle-tendon system for phalange motion under desired trajectory profiles, by actuating the muscle-tendon system through the virtual CNS control. A simplified system analogous to the actual biomechanical system is proposed here for the development of the model. The authors propose a model of the phalange structure, with associated muscle-tendon units actuating it, for desired motion through a virtual phalange system.

The concept is explained in detail for a simpler case by considering a single phalange in motion. The authors have considered one of the phalanges of the hand, which is to be actuated through MTUs. A virtual and a real domain are considered for modeling the musculoskeletal actuation system. The virtual domain refers to the CNS consisting of a virtual phalange and associated virtual MTCs. The virtual phalange is considered with the same nominal specifications as that of the real phalange. The virtual phalange is moved along the desired trajectory given as an input to its tip but is not actuated through any muscle-tendon unit. The desired trajectory at the tip of the virtual phalange, imposed through stiffness and damping elements, provides appropriate force at its tip to impart desired motion. For the real phalange to track the virtual phalange, the MTCs need the information of instantaneous velocities at corresponding points from the virtual and real phalanges. For this purpose, a control strategy for the MTCs is needed, which acquires the information, computes the error, and actuates the real muscle-tendon system.

Figure 1 shows the details of the muscle-tendon actuation system of the phalange. On the left side, there is a virtual phalange and a real phalange is on the right. A body frame is fixed at the bottom center of each phalange, which initially coincides with the inertial frame $\{0\}$. Body frames $\{1_v\}$ and $\{1\}$ are assigned for the virtual and real phalanges, respectively. The dorsal, distal, and radial directions are considered along the X_0, Y_0, and Z_0 – axes, respectively, in the inertial frame. The real phalange is considered to be connected to four MTUs placed at symmetrical locations. Originating locations of the muscle tendons and their insertions on the real and virtual phalanges are shown in Fig. 1 as H, P
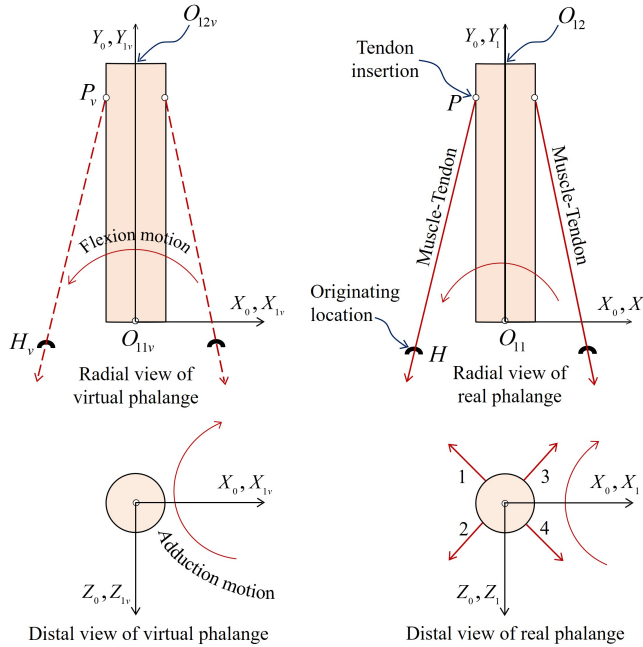
Fig. 1. Virtual and real phalange showing details of motions and muscle-tendon units attached.

and H_v, P_v respectively. Only one tendon insertion and one originating location for a muscle tendon are shown to avoid clutter.

Each MTU is made to pass through its corresponding tendon originating location, which is fixed with respect to the inertial frame. The direction of the actuation force by the MTU that needs to be applied on the real phalange is along the line joining its originating location with its point of insertion. The stimulus required for the activation of the MTUs is obtained from the corresponding MTCs. Each MTU performs its function only when in tension, as there is no generation of force in its slackened state. In order to maintain a taut condition in the MTUs, there is always some pre-tension in the natural musculoskeletal system of the human body. For this essentiality, the role of pre-tension has also been incorporated in the model developed for muscle-tendon actuation. A detailed control scheme for muscle-tendon actuation is described in Subsec. 2.1 below.

2.1. Control scheme for the muscle-tendon actuation system

In real-life biomechanical systems, every locomotion to be performed by the body requires initiation at the level of the CNS. It is considered that initially, an intent is generated for the desired motion. The CNS senses the actual instantaneous position of the limb. Based on the information of the actual position and

desired position of the limb, the CNS estimates the joint angles required. The CNS stimulates and sends specific control signals through the network of nerves to the corresponding skeletal muscles for the required muscle-tendon actuation to move the limb. In this research, a control strategy to emulate the role of the CNS has been developed specifically for the phalange motion. The detailed structure of the system is described below and depicted in Fig. 4.

A desired virtual trajectory, i.e., the desired motion input (flow) based on the desired task, is applied to the tip of the imaginary virtual phalange. Based on this trajectory, the posture and joint angle of the virtual phalange are determined.

The information of velocities from the tendon insertion location of the MTU is obtained from the real phalange and the corresponding location on the virtual phalange. A virtual MTC, as a part of CNS, provides the necessary activation to the muscle-tendon structure connected to the real phalange. The virtual MTC compares these velocities to compute the error in velocities $\dot{\varepsilon}(t)$, which upon integration yields the tip trajectory error, $\varepsilon(t)$. Corresponding to this error $\varepsilon(t)$, the MTC generates muscle activation force. This force is given as an input to the MTU through a point mass δm connected at the free end of the MTU. The point mass δm determines the velocity at the free end of the MTU. Due to which motion-specific extension patterns are produced in the elements of the muscle tendons. Corresponding to these extension patterns, the model determines the required forces that need to be applied by the muscle-tendon mechanism. Comparing the velocities at the free end of the MTU with the corresponding velocity at the respective tendon insertion location on the real phalange, the MTU generates a corresponding force profile based on its nonlinear characteristics. This force is applied at the respective insertion location on the real phalange.

This control strategy is applied to all the MTUs simultaneously. The corresponding force profiles are generated by all the connected muscle tendons to actuate the dynamics of the real phalange. Consequently, the required joint torques are determined to move the real phalange to the desired trajectory. Before discussing the complete mechanics for the proposed model using the bond graph, it is essential to understand the mechanics and modeling of the MTU.

2.2. Mechanics and modeling of the muscle-tendon unit (MTU)

Skeletal muscles are one of the major constituents of the human body and are the prime mover for locomotion [16]. The viscoelastic characteristics of skeletal muscles are nonlinear and strain dependent. The high strength of these muscles enables the body to hold high loads under tensile conditions. The muscle-tendon unit is modeled using a well-developed concept based on modified four-element Hill's muscle model [2, 16], as shown in Fig 2, and its detailed bond graph model is shown in Fig. 3 [11].
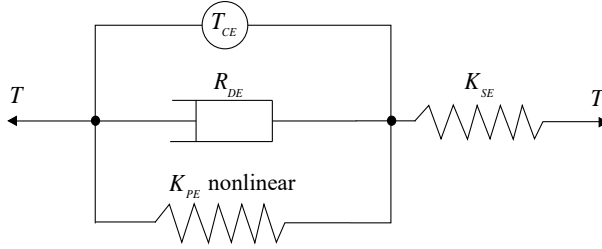
FIG. 2. Physical model of Hill's four-element muscle model (MTU).

Here, T_{CE} is the contractile element, which develops the force during active movement. The contractile force is an internal force developed by the muscle. This element does not contribute any force to the system during passive motion or resting position. The contractile elements in each muscle tendon contract to pull their respective associated tendons so as to move the phalange. The force required to pull each tendon connected to the phalange is provided by the internal mechanochemical mechanism of the contractile elements at the tissue level. Here, a passive system of actuation is used to study the behavior of the system in which the role of T_{CE} is not considered. The passive property is dependent on the strain. We focus exclusively on the aspect of determination of forces and extension patterns developed in the muscle tendons for a given movement.

Next, K_{PE} is the parallel elastic (PE) member representing a soft connective tissue network that resists passive stretching in the muscles. It has a strain-dependent nonlinear behavior, as presented in (1), which is important to consider when predicting muscle forces during dynamic loading [2]:

$$F_{PE} = 0.00163(\exp^{7.66\epsilon} -1), \tag{1}$$

where F_{PE} is the force developed by the nonlinear element K_{PE} during stretching and ϵ represents the corresponding strain in the muscle. Figures 3a and 3b show the bond graph of Hill's muscle model and the nonlinear characteristic of the parallel-elastic member, respectively.

The resistive element R_{DE} is a dynamic viscous damping element whose characteristics are unspecified in the literature. We assume a linear relationship for the viscous damping element between the force and the strain rate across the PE element, as exact characteristics are not available. The fourth element in Hill's muscle model is a series-elastic element K_{SE} that represents the muscle-tendon interface with the phalange for transmitting the force to the phalange. The value of K_{SE} is much stiffer than that of K_{PE}, and its corresponding relation between tension and extension is linear. Based on the extension of the series-elastic (SE) element, a force is determined by the MTU given in (2). The muscle activation is provided at the free end of the respective MTU and is transmitted to the tendon

a)
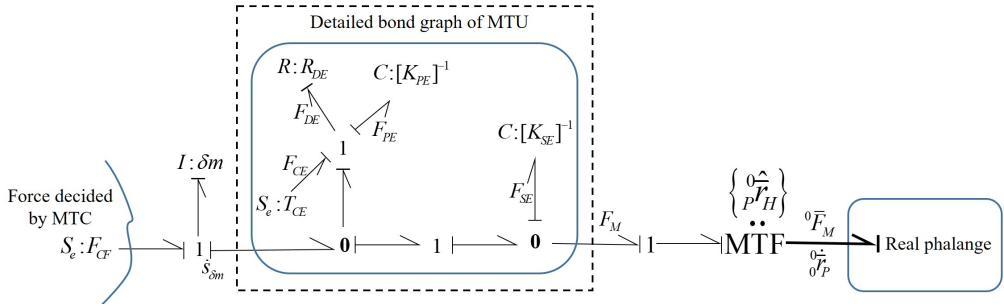
b)
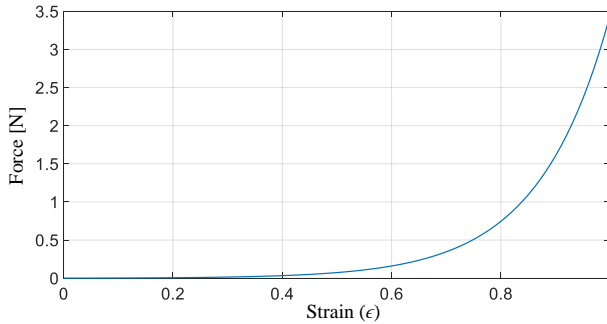
FIG. 3. a) Bond graph of Hill's muscle model, b) characteristic of PE member K_{PE} vs. strain.

insertion point on the real phalange. The force transmitted through the MTU is given as:

$$F_M = F_{SE} = F_{CE} + F_{PE} + F_{DE}, \qquad (2)$$

where F_{SE} is the force developed at the respective series-elastic element which is to be transmitted to the real phalange through the tendon interface. The force developed by the contractile element is taken as zero, i.e., $F_{CE} = 0$, as a passive actuation is considered. F_{DE} is the damping force from the resistive element, and F_{PE} is the force developed by the nonlinear PE element K_{PE}. Description of the MTU mechanics, the proposed model for the motion of the phalange through it, is explained in detail in Sec. 3 using the bond graph.

3. MULTIBOND GRAPH MODEL FOR THE ACTUATION OF PHALANGE BY MUSCLE–TENDON

To explain the proposed model, a detailed multibond graph model based on rigid body dynamics for the phalange actuated by viscoelastic muscle tendons is presented, as shown in Fig. 4. Scalar bonds are represented using thin lines, and multibonds with a cardinality of 3, with thick lines.
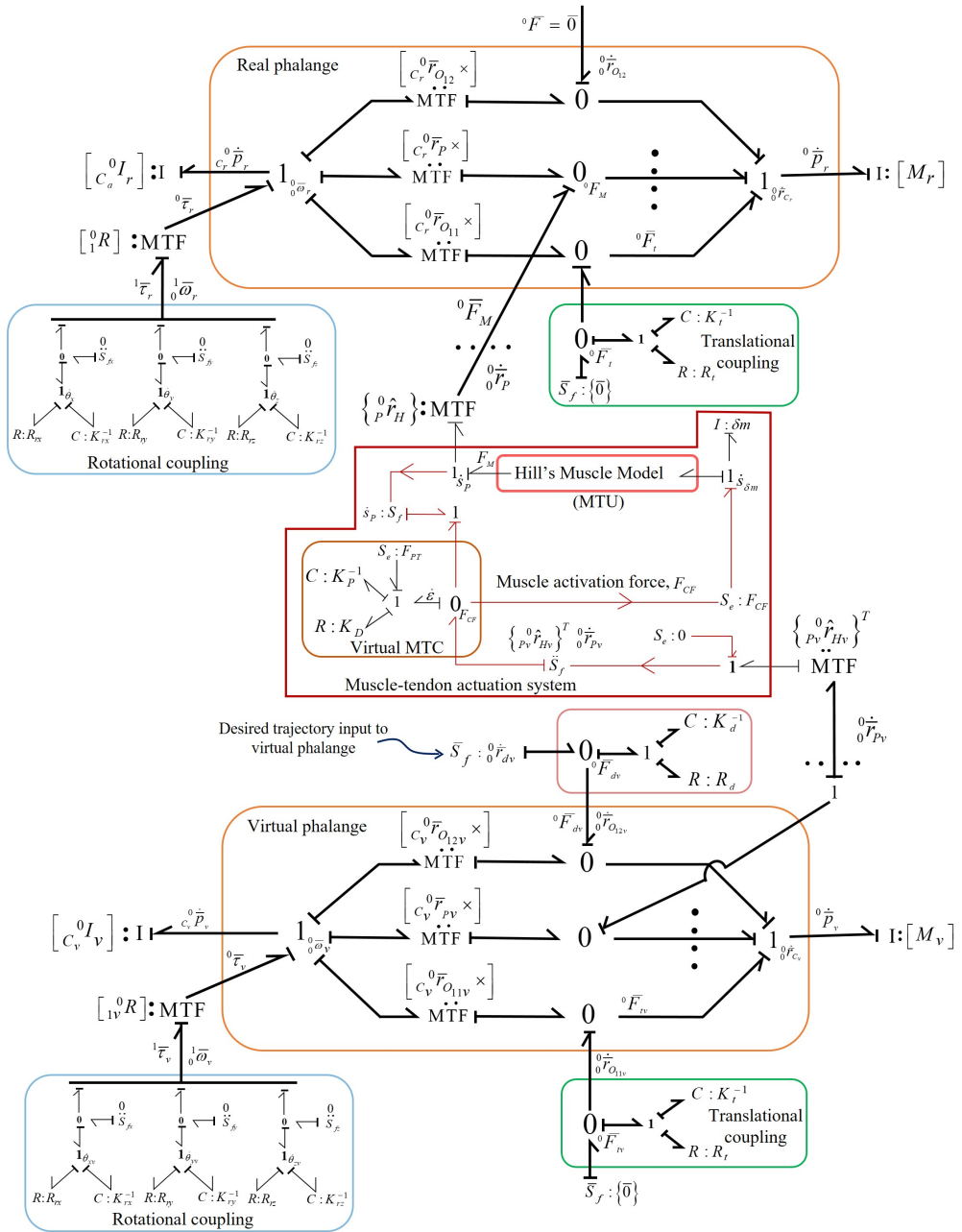
FIG. 4. Bond graph model of virtual and real phalange with MTU and virtual MTC.

The basic task to be performed is to move the real phalange so as to track the desired motion trajectory. The bond graph model representing the complete

dynamics of the system, including the virtual phalange and associated MTCs as a part of the CNS, generating commands for the actuation of the real phalange by corresponding connecting MTUs, is depicted in Fig. 4. To avoid clutter only one of the MTUs with the real phalange is shown in the bond graph. A similar approach is applied to all the MTUs.

The desired motion trajectory is given as an input to the tip O_{12v} of the virtual phalange. Corresponding to this desired trajectory, a velocity profile $^0_0\dot{\overline{r}}_{dv}$ is imposed at the tip of the virtual phalange by a source of the flow $\overline{S}_f : {}^0_0\dot{\overline{r}}_{dv}$. However, this has to be realized by applying a force at the tip. This force is transmitted through a coupling subsystem of elements $C : K_d^{-1}$ and $R : R_d$. The force $^0\overline{F}_{dv}$, required to maintain the desired motion of the virtual phalange, is determined by the connected coupling subsystem, as shown in Fig. 4. This force is common to all the bonds at the $0_{0\overline{F}_{dv}}$ junction.

After that, velocity information $^0_0\dot{\overline{r}}_{Pv}$ and $^0_0\dot{\overline{r}}_P$ at the tendon insertion locations P_v and P are taken from the virtual and real phalanges, respectively. It is required to resolve this velocity information along the direction of the MTU, as the MTU is considered as a one-dimensional unit. This is obtained using modulated transformer elements MTF : $\left\{ {}^0_P\widehat{\overline{r}}_H \right\}$ and MTF : $\left\{ {}^0_{Pv}\widehat{\overline{r}}_{Hv} \right\}$ in the form of unit vectors directed along the directions of the MTU on the real and virtual phalanges, respectively. The moduli of these MTF elements keep on changing with the posture of the phalange. Accordingly, the direction of the force applied by the MTU on the real phalange changes. The MTC receives this velocity information directed along the MTU via the sources of the flow $S_f : \left\{ {}^0_{Pv}\widehat{\overline{r}}_{Hv} \right\}^T {}^0_0\dot{\overline{r}}_{Pv}$ and $S_f : \dot{s}_P$ from the corresponding virtual and real phalanges. Next, the MTC compares this information of velocity at the $0_{F_{CF}}$ junction to determine the error in velocities $\dot{\varepsilon}(t)$. Upon integration with regard to time t, it yields the error $\varepsilon(t)$. The virtual MTC determines a force proportional to this error through the elements $C : K_P^{-1}$ and the error derivative through the elements $R : R_D$ connected to it, as depicted in Fig. 4. This force, along with the pre-tension force F_{PT}, determines a controller force F_{CF} applied as a source of effort by $S_e : F_{CF}$. This force F_{CF} activates the muscle dynamics of the MTU through the point mass δm connected at the free end of the MTU on the $1_{\dot{s}_{\delta m}}$ junction. Based on this muscle activation, the momentum of the point mass δm changes, and velocity $\dot{s}_{\delta m}$ acts upon the free end of the MTU as represented at the $1_{\dot{s}_{\delta m}}$ junction for the excursion of the muscle tendon. Velocity $\dot{s}_{\delta m}$ from the point mass δm and velocity $\dot{s}_P$ at the corresponding insertion location P on the real phalange are inputs to the MTU structure.

The difference of these two velocities, which corresponds to the muscle extension, decides the amount of force F_M generated in the MTU based on its nonlinear behavior, as given in (2). The force F_M developed is thus applied at

the insertion location P on the real phalange through MTF: $\left\{ {}^{0}_{P}\widehat{\overline{r}}_{H} \right\}$, resulting in the force ${}^{0}\overline{F}_{M}$, as shown in Fig. 4.

As a result, the required moments are generated at the real phalange joint to move the real phalange. In this way, the real phalange follows the desired trajectory profile so as to track the virtual phalange. The system equations for the mechanics of the bond graph model are explained in detail below.

3.1. System equations

System equations are derived algorithmically from the bond graph model itself according to the procedure explained in detail in [17].

3.1.1. Translational motion of the virtual and real phalanges. The joint interface is modeled with a translational coupling consisting of compliance and resistive elements, i.e., $C : K_t^{-1}$ and $R : R_t$ elements, to account for the flexibility of the joint (ref. bond graph model in Fig. 4). Various forces exerted by the subsystems acting on the phalange contribute to the rate of change of the translational momentum of the phalange, ${}^{0}_{0}\dot{\overline{r}}_{Cv}$ represents the translational velocity of the center of mass (COM) of the virtual phalange observed and expressed in the inertial frame $\{\boldsymbol{0}\}$ and is represented in the bond graph by the $\mathbf{1}_{{}^{0}_{0}\dot{\overline{r}}_{Cv}}$ junction, and ${}^{0}\overline{p}_v$ is the translational momentum of the virtual phalange considering the mass to be concentrated at its center of gravity, observed and expressed in the inertial frame $\{\boldsymbol{0}\}$. The rate of change of translational momentum is

$$\frac{d}{dt}\left\{ {}^{0}\overline{p}_v \right\} = {}^{0}\overline{F}_{tv} + {}^{0}\overline{F}_{dv}, \tag{3}$$

where ${}^{0}\overline{F}_{tv}$ is the reaction force applied by the translational coupling between the virtual phalange and the ground, ${}^{0}\overline{F}_{dv}$, is the effort applied on the tip of the virtual phalange for the desired virtual motion, and $\left\{ {}^{0}\overline{p}_v \right\} = M_v \left\{ {}^{0}_{0}\dot{\overline{r}}_{Cv} \right\}$ is the translational momentum.

Similarly, the system equations for the translational motion of the real phalange are derived as:

$$\frac{d}{dt}\left\{ {}^{0}\overline{p}_r \right\} = {}^{0}\overline{F}_t + {}^{0}\overline{F}_M, \tag{4}$$

where ${}^{0}\overline{F}_t$ is the reaction force applied by the translational coupling between the real phalange and the ground, ${}^{0}\overline{F}_M$ is the force applied by the MTU on the insertion location of the tendon on the real phalange, and $\left\{ {}^{0}\overline{p}_r \right\} = M_r \left\{ {}^{0}_{0}\dot{\overline{r}}_{Cr} \right\}$ is the translational momentum of the real phalange. The force developed by the MTU is explained in detail in the following section.

3.1.2. Rotational motion of the virtual phalange. A symbol ${}_0^0\overline{\omega}_v$ represents the angular velocity of the COM of the virtual phalange observed and expressed in the inertial frame $\{0\}$ and is represented in the bond graph by the $\mathbf{1}_{{}_0^0\overline{\omega}_v}$ junction.

This junction also performs a summation of various moments about the COM of the virtual phalange as:

$$\frac{d}{dt}\left\{{}_{C_v}^0\overline{p}_v\right\} = {}^0\overline{\tau}_v - \left[{}_{C_v}^0\overline{r}_{O_{11v}}\times\right]^T {}^0\overline{F}_{tv} - \left[{}_{C_v}^0\overline{r}_{O_{12v}}\times\right]^T {}^0\overline{F}_{dv}, \tag{5}$$

where ${}^0\overline{\tau}_v$ is the torque applied by the rotational coupling of the virtual phalange, $-\left[{}_{C_v}^0\overline{r}_{O_{11v}}\times\right]^T {}^0\overline{F}_{tv} = \left[{}_{C_v}^0\overline{r}_{O_{11v}}\times\right] {}^0\overline{F}_{tv}$ is the moment exerted on the virtual phalange about its COM by the external force ${}^0\overline{F}_{tv}$ due to the translational coupling at O_{11v}, and $-\left[{}_{C_v}^0\overline{r}_{O_{12v}}\times\right]^T {}^0\overline{F}_{dv} = \left[{}_{C_v}^0\overline{r}_{O_{12v}}\times\right] {}^0\overline{F}_{dv}$ is the moment on the virtual phalange about its COM by the external force due to the translational coupling between the phalange tip and the imposed desired motion input.

Futhermore, MTF: $\left[{}_{C_v}^0\overline{r}_{O_{11v}}\times\right]$ is a modulated multibond transformer that keeps on changing with the orientation of the phalange and is a skew-symmetric matrix obtained from the position vector ${}_{C_v}^0\overline{r}_{O_{11v}} = \left\{{}_{C_v}^0 x_{O_{11v}} \quad {}_{C_v}^0 y_{O_{11v}} \quad {}_{C_v}^0 z_{O_{11v}}\right\}^T$, representing the position of the point O_{11v} on the virtual phalange with respect to the COM C_v of the virtual phalange, observed and expressed in the frame $\{0\}$ as:

$$\left[{}_{C_v}^0\overline{r}_{O_{11v}}\times\right] = \begin{bmatrix} 0 & -{}_{C_v}^0 z_{O_{11v}} & {}_{C_v}^0 y_{O_{11v}} \\ {}_{C_v}^0 z_{O_{11v}} & 0 & -{}_{C_v}^0 x_{O_{11v}} \\ -{}_{C_v}^0 y_{O_{11v}} & {}_{C_v}^0 x_{O_{11v}} & 0 \end{bmatrix}. \tag{6}$$

The other skew-symmetric matrices are evaluated similarly.

The angular momentum of the virtual phalange about its center of mass, expressed in the inertial frame $\{0\}$, and represented by ${}_{C_v}^0\overline{p}_v$ is given as

$$_{C_v}^0\overline{p}_v = \left[{}_{C_v}^0 I_v\right] {}_0^0\overline{\omega}_v, \tag{7}$$

where $\left[{}_{C_v}^0 I_v\right]$ represents the inertia tensor of the virtual phalange about its center of mass, expressed in the frame $\{0\}$.

3.1.3. Rotational motion of the real phalange. Similarly, the system equations for the rotational motion of the real phalange can be determined. The angular velocity of the real phalange observed and expressed in the inertial frame $\{0\}$ and represented in the bond graph by the $\mathbf{1}_{{}_0^0\overline{\omega}_r}$ junction is ${}_0^0\overline{\omega}_r$. The summation of the various moments acting about its COM on the real phalange result in the change of its angular momentum as:

$$\frac{d}{dt}\left\{{}^0_{C_r}\bar{p}_r\right\} = {}^0\bar{\tau}_r - \left[{}^0_{C_r}\bar{r}_{O_{11}}\times\right]^T {}^0\bar{F}_t - \left[{}^0_{C_r}\bar{r}_{O_P}\times\right]^T {}^0\bar{F}_M, \tag{8}$$

where ${}^0\bar{\tau}_r$ is the torque applied by the rotational coupling of the real phalange, $-\left[{}^0_{C_r}\bar{r}_{O_{11}}\times\right]^T {}^0\bar{F}_t = \left[{}^0_{C_r}\bar{r}_{O_{11}}\times\right] {}^0\bar{F}_t$ is the moment exerted on the real phalange about its COM by external forces ${}^0\bar{F}_t$ due to the translational coupling between the real phalange and the ground, $-\left[{}^0_{C_r}\bar{r}_{O_P}\times\right]^T {}^0\bar{F}_M = \left[{}^0_{C_r}\bar{r}_{O_P}\times\right] {}^0\bar{F}_M$ represents the moment acting on the real phalange about its COM due to the actuation force ${}^0\bar{F}_M$ provided by the MTU at the tendon insertion location P, MTF: $\left[{}^0_{C_r}\bar{r}_{O_{11}}\times\right]$ and MTF: $\left[{}^0_{C_r}\bar{r}_{O_P}\times\right]$ are modulated multibond transformers, and ${}^0_{C_r}\bar{p}_r$ represents the angular momentum of the real phalange about its COM, expressed in the inertial frame $\{\boldsymbol{0}\}$, given by

$$ {}^0_{C_r}\bar{p}_r = \left[{}^0_{C_r}I_r\right] {}^0_0\bar{\omega}_r, \tag{9}$$

where $\left[{}^0_{C_r}I_r\right]$ represents the inertia tensor of the real phalange about its COM expressed in the frame $\{\boldsymbol{0}\}$.

3.1.4. Rotational couplings. The joint at the phalange is modeled as a revolute joint. The joint provides the necessary rotational constraint for the rotation of the phalange through the viscoelastic rotational coupling. A detailed bond graph for the rotational coupling has been shown in Fig. 4. Angular velocity of the revolute joint at the virtual phalange, observed with respect to the inertial frame $\{\boldsymbol{0}\}$ and expressed in the body frame $\{\boldsymbol{1}\}$, can be related as:

$$ {}^{1v}_0\bar{\omega}_v = {}^0_{1v}R^T {}^0_0\bar{\omega}_v, \tag{10}$$

where ${}^0_0\bar{\omega}_v$ is the angular velocity of the virtual phalange, observed and expressed in the frame $\{\boldsymbol{0}\}$, ${}^{1v}_0\bar{\omega}_v$ consists of three mutually orthogonal components in the x, y, and z directions in the body frame $\{\boldsymbol{1_v}\}$. The corresponding moments are developed in these directions by the associated rotational stiffness elements $C : K_{rx}^{-1}$, $C : K_{ry}^{-1}$, $C : K_{rz}^{-1}$ and rotational damping elements $R : R_{rx}$, $R : R_{ry}$, $R : R_{rz}$ of the rotational couplings that oppose the relative motion at the joint. The components of the torque developed at the rotational coupling can be written as:

$$ {}^{1v}\tau_{xv} = K_{rx}\theta_{xv} + R_{rx}\dot{\theta}_{xv}, $$

$$ {}^{1v}\tau_{yv} = K_{ry}\theta_{yv} + R_{ry}\dot{\theta}_{yv}, \tag{11}$$

$$ {}^{1v}\tau_{zv} = K_{rz}\theta_{zv} + R_{rz}\dot{\theta}_{zv}, $$

$$ {}^1\bar{\tau}_v = \left\{{}^{1v}\tau_{xv} + {}^{1v}\tau_{yv} + {}^{1v}\tau_{zv}\right\}, $$

$$ {}^0\bar{\tau}_v = {}^0_{1v}R\left\{{}^{1v}\tau_{xv} + {}^{1v}\tau_{yv} + {}^{1v}\tau_{zv}\right\}, \tag{12}$$

where ${}^{1v}\tau_{xv}$, ${}^{1v}\tau_{yv}$ and ${}^{1v}\tau_{zv}$ represent the components of the torque in the x, y, and z directions expressed in the frame $\{\boldsymbol{1_v}\}$, and $\dot{\theta}_{xv}$, $\dot{\theta}_{yv}$, and $\dot{\theta}_{zv}$ are the components of the angular velocity in the x, y, and z directions, respectively, and ${}^{0}_{1v}R$ represents the rotational transformation matrix from the frame $\{\boldsymbol{1_v}\}$ to the inertial frame $\{\boldsymbol{0}\}$. The time rate of change of the rotation matrix is expressed as:

$$ {}^{0}_{1v}\dot{R} = \left[{}^{0}_{0}\overline{\omega}_v\times\right]{}^{0}_{1v}R. \tag{13} $$

The initial orientation of the virtual phalange determines the initial value of ${}^{0}_{1v}R$ with respect to the inertial frame $\{\boldsymbol{0}\}$.

Similarly, the system equations for the rotational couplings at the real phalange are derived as:

$$ {}^{0}\overline{\tau}_r = {}^{0}_{1}R\left\{{}^{1}\tau_x + {}^{1}\tau_y + {}^{1}\tau_z\right\}, \tag{14} $$

where ${}^{1}\tau_x$, ${}^{1}\tau_y$ and ${}^{1}\tau_z$ represent the components of the torque in the x, y, and z directions, respectively, expressed in the frame $\{\boldsymbol{1}\}$, and ${}^{0}_{1}R$ represents the rotational transformation matrix from the frame $\{\boldsymbol{1}\}$ to the inertial frame $\{\boldsymbol{0}\}$. The time rate of change of the rotation matrix is expressed as:

$$ {}^{0}_{1}\dot{R} = \left[{}^{0}_{0}\overline{\omega}_r\times\right]{}^{0}_{1}R. \tag{15} $$

The initial orientation of the real phalange determines the initial value of ${}^{0}_{1}R$ with respect to the inertial frame $\{\boldsymbol{0}\}$.

3.1.5. Virtual muscle-tendon controller (MTC) and muscle-tendon units (MTU). The CNS activates the dynamics of the muscle-tendon unit by sending the control signals through the network of nerves to the corresponding muscle tendon for the required actuation of the phalange [2, 16]. Accordingly, the muscle tendon generates the required force to bring the phalange into motion. The CNS is emulated for controlling the motion of the real phalange. The control scheme for obtaining the movement of the real phalange system so as to track the desired trajectory observed from the virtual system is elaborated in detail in Subsec. 2.1. The control scheme is explained here in detail from a bond graph perspective.

The translational velocities of the COM of the virtual and the real phalanges are represented by ${}^{0}_{0}\dot{\overline{r}}_{C_v}$ and ${}^{0}_{0}\dot{\overline{r}}_{C_r}$, respectively, as observed and expressed in the inertial frame, ${}^{0}_{0}\overline{\omega}_v$ and ${}^{0}_{0}\overline{\omega}_r$ represent the angular velocities of the COM of the virtual and real phalanges, respectively, as observed and expressed in the inertial frame. The translational velocities ${}^{0}_{0}\dot{\overline{r}}_{Pv}$ and ${}^{0}_{0}\dot{\overline{r}}_{P}$ at the tendon insertion

locations, for virtual and real phalanges, respectively, are related to the corresponding angular velocities of the phalanges using kinematic relationships as:

$$
\begin{aligned}
{}_0^0\dot{\bar{r}}_{Pv} &= {}_0^0\dot{\bar{r}}_{C_v} - \left[{}_{C_v}^0\bar{r}_{Pv}\times\right] {}_0^0\bar{\omega}_v, \\
{}_0^0\dot{\bar{r}}_P &= {}_0^0\dot{\bar{r}}_{C_r} - \left[{}_{C_r}^0\bar{r}_P\times\right] {}_0^0\bar{\omega}_r,
\end{aligned}
\tag{16}
$$

where $\left[{}_{C_v}^0\bar{r}_{Pv}\times\right]$ and $\left[{}_{C_r}^0\bar{r}_P\times\right]$ are the moduli of the respective modulated multibond transformers and are skew-symmetric matrices obtained from position vectors ${}_{C_v}^0\bar{r}_{Pv} = \left\{{}_{C_v}^0 x_{Pv} \quad {}_{C_v}^0 y_{Pv} \quad {}_{C_v}^0 z_{Pv}\right\}^T$ and ${}_{C_r}^0\bar{r}_P = \left\{{}_{C_r}^0 x_P \quad {}_{C_r}^0 y_P \quad {}_{C_r}^0 z_P\right\}^T$, respectively. The difference between the two velocities ${}_0^0\dot{\bar{r}}_{Pv}$ and ${}_0^0\dot{\bar{r}}_P$ at the corresponding virtual and real phalange is compared in a direction along the length of the muscle tendon, as the MTU is considered a one-dimensional element. The error velocity $\dot{\varepsilon}(t)$ is determined by the MTU controller, and a corresponding force F_{CF} is generated as:

$$
\dot{\varepsilon}(t) = \left\{{}_{Pv}^0\widehat{r}_{Hv}\right\}^T {}_0^0\dot{\bar{r}}_{Pv} - \left\{{}_P^0\widehat{r}_H\right\}^T {}_0^0\dot{\bar{r}}_P,
\tag{17}
$$

$$
F_{CF} = K_P\varepsilon + R_D\dot{\varepsilon} + F_{PT},
\tag{18}
$$

where ${}_P^0\widehat{r}_H$ is the unit vector describing the direction along which the force is applied to the real phalange at the tendon insertion location P on the real phalange, and ${}_{Pv}^0\widehat{r}_{Hv}$ is the corresponding unit vector in the virtual system. As the force is needed to be applied along the line of the tendon, a straight-line connection is considered between the muscle-tendon insertion P and the originating location H, as shown in Fig. 1. Here, F_{CF} is the force determined by the MTC proportional to the error through the elements K_P and the error derivative through the elements R_D connected to it, as described in Fig. 4, and F_{PT} is the pre-tension force applied to the MTU by the MTC in order to maintain the muscle tendon in a taut state. The force F_{CF} activates the dynamics of the MTU through the point mass δm. Based on the muscle activation, the MTU determines the forces as:

$$
F_{SE} = K_{SE}q_{SE},
\tag{19}
$$

$$
F_{DE} = F_{SE} - F_{PE} - F_{CE},
\tag{20}
$$

$$
\dot{q}_{SE} = \dot{s}_{\delta m} - \frac{F_{DE}}{R_{DE}} - \left\{{}_P^0\widehat{r}_H\right\}^T {}_0^0\dot{\bar{r}}_P,
\tag{21}
$$

where $\dot{q}_{SE}$ is the flow obtained in the series-elastic element of the MTU, which upon integration yields the deformation in it as q_{SE}. The MTC applies the muscle activation force only if the condition $q_{SE} > 0$ is satisfied, i.e., the muscle

is able to apply force during tension only when the muscle is being pulled. When $q_{SE} \leq 0$, the force applied by the MTU to the real phalange is zero. This means there is no transmission of force by the MTU when in a slackened or unstretched condition.

Forces F_{PE}, F_{SE} and F_{DE} are the forces developed in the PE element, series-elastic element, and damping element of the MTU, respectively. The force F_{CE} from the active contractile element is taken as zero here, as only passive actuation is considered, and $\dot{s}_{\delta m}$ is the speed of the point mass along the length of the tendon. The series-elastic element stretches out and generates the force F_{SE} that is applied at the insertion location of the tendon unit on the real phalange, along with the pre-tension force F_{PT}, resulting in a force F_M.

The same procedure is followed for obtaining system equations for all the MTUs. The forces generated by all the MTUs based on their extension patterns are determined and summed up to obtain the rate of change of linear momentum and angular momentum of the real phalange as:

$$\frac{d}{dt}\left\{{}^0\overline{p}_r\right\} = {}^0\overline{F}_t + \sum_{i=1}^{4}\overline{F}_{Mi}, \tag{22}$$

$$\frac{d}{dt}\left\{{}^0_{C_r}\overline{p}_r\right\} = {}^0\overline{\tau}_r - \left[{}^0_{C_r}\overline{r}_{O_{11}}\times\right]^T {}^0\overline{F}_t - \sum_{i=1}^{4}\left[{}^0_{C_r}\overline{r}_{O_{Pi}}\times\right]^T {}^0\overline{F}_{Mi}, \tag{23}$$

where ${}^0\overline{F}_t$ is the force due to translational coupling, ${}^0\overline{\tau}_r$ is the torque applied by the rotational coupling, ${}^0\overline{F}_{Mi}$ is the force applied by the MTUs at the tendon insertion locations, with i varying from 1 to 4, as four MTUs are considered for describing the model.

The model is simulated for some general motions of flexion-extension, adduction-abduction, and circumduction. Simulation results for the three cases are discussed in the succeeding section.

4. Simulation and discussion

4.1. Initial conditions and simulation parameters

The bond graph model of the muscle-tendon actuation system for the phalange, for three-dimensional motion, is simulated. General motions such as flexion-extension, adduction-abduction, and circumduction are considered here to study the behavior of the real system for given trajectories. Simulation code is written from the bond graph model itself using MATLAB.

The phalange is considered as a cylindrical body with uniform density throughout its length, just as an example to demonstrate the conceptual model of the

system dynamics. However, the model presented can be used for any geometrical shape. The location of the center of mass of the phalange, and the inertia tensor about its center of mass, expressed in the body frame, are important for the analysis of the system. The physical parameters of the virtual and real phalange are adapted as the length $l_v = l_r = 40$ mm and radius of the phalange $r_v = r_r = 5$ mm [18–21]. The radius is taken at the plane of minimal shaft cross-section well away from the head and base enlargements of the phalange. The density of the bone varies non-uniformly across the body. It ranges from 0.1–1.85 g/cc from trabecular to cortical bone [22, 23]. The mass of the phalange $m_v = m_r = 5.5$ g is determined by using the density of the bone as 1.75 g/cc. The inertial properties are listed in Table 1.

TABLE 1. Inertial properties of the phalanges.

Phalange	Direction	Moment of inertia	Moment of inertia $[\text{kg} \cdot \text{m}^2]$
Virtual and real phalange	X	$I_{xx} = \dfrac{m}{2}\left(l^2 + 3r^2\right)$	$I_{xxr} = I_{xxv} = 7.6771 \times 10^{-7}$
	Y	$I_{yy} = \dfrac{m}{2}\left(r^2\right)$	$I_{yyr} = I_{yyv} = 6.8750 \times 10^{-8}$
	Z	$I_{zz} = \dfrac{m}{2}\left(l^2 + 3r^2\right)$	$I_{zzr} = I_{zzv} = 7.6771 \times 10^{-7}$

Stiffness and damping elements in the system govern the translational and rotational couplings at the joint. The joint properties of the translational and rotational stiffness and their corresponding damping parameters are listed in Table 2. The properties of the elements of Hill's muscle model are adapted as $K_{SE} = 160$ kN/m [24]; R_{DE}, the damping characteristic value is considered as 1 N·s/m. We assume a linear relationship for the viscous damping element between the force and the strain rate across the PE element, as exact characteristics are not available. We have simulated the system using various parametric values of R_{DE}. The characteristics of the PE element K_{PE} is specified as non-linear, as depicted in (1). The parameters for imposing the desired trajectory for the motion are taken as: $K_d = 1 \times 10^3$ N/m and $R_d = 5$ N·s/m. The gains of the virtual MTC corresponding to its error and error derivative elements K_P and K_D are taken as 6.7×10^3 N/m and 20 N·s/m for flexion-extension and adduction-abduction motion, respectively. The corresponding gains of the MTC for the circumduction motion are taken as 50 N/m and 5 N·s/m, respectively.

Providing the desired trajectory is the task of the CNS, the role of such a trajectory is emulated next. The trajectories applied to the system are smooth and jerk-free to behave as natural phalange. This is also desirable from nature's perspective to prevent injury [25]. The controlled trajectory profiles are applied at the tip of the virtual phalange to impart desired motion. Initially, a pre-

tension is applied through the MTC to all the MTUs of the real phalange. The system is then kept under the state of pre-tension for 10 s in flexion-extension and adduction-abduction motion to attain equilibrium. After that, an angular trajectory profile is imposed on the virtual phalange for flexion-extension or adduction-abduction motion for the next 10 s. There is a dwell of 20 s, after which it is brought back finally to its initial posture in the next 10 s. The results for the flexion-extension and adduction-abduction motion are discussed in Subsecs. 4.2.1 and 4.2.2, respectively. The circumduction motion trajectory is explained separately in Subsec. 4.2.3.

Equation (24) represents the generalized basis on which desired trajectory is formulated for the desired motion. The virtual phalange starts moving from an initial position $\theta_d(t_i) = 0$ up to $\theta_d(t_f) = \theta_{df}$. As the phalange is considered a rigid body, with the change in the x-coordinate, the y-coordinate of the tip also changes. To prevent transients at the start and finish of the motion and to provide a smooth trajectory, the velocity $\dot{\theta}_d(t)$, acceleration $\ddot{\theta}_d(t)$, and jerk $\dddot{\theta}_d(t)$ components are zero at the starting and ending time of the desired motion. The generalized trajectory profile for the motion is taken as:

$$\theta_d(t) = 0, \quad t \leq 0,$$

$$\theta_d(t) = a_0 + a_1 t + a_2 t^2 + a_3 t^3 + a_4 t^4 + a_5 t^5 + a_6 t^6 + a_7 t^7, \quad 0 \leq t \leq t_f, \quad (24)$$

$$\theta_d(t) = \theta_{df}, \quad t > t_f,$$

where $a_0, a_1, ..., a_7$ are coefficients of the polynomial and are obtained by applying the boundary conditions at the initial and final positions.

At $t = t_0$,

$$\theta_d(t_0) = 0, \quad \dot{\theta}_d(t_0) = 0, \quad \ddot{\theta}_d(t_0) = 0, \quad \dddot{\theta}_d(t_0) = 0.$$

At $t = t_f$,

$$\theta_d(t_f) = \theta_{df}, \quad \dot{\theta}_d(t_f) = 0, \quad \ddot{\theta}_d(t_f) = 0, \quad \dddot{\theta}_d(t_f) = 0.$$

The desired trajectory profile is applied to rotate the phalange about the inertial Z_0-axis for flexion-extension motion, and the trajectory profile for the adduction-abduction motion is applied about the inertial X_0-axis.

The proposed model simulated for three different cases of motion: flexion-extension, adduction-abduction, and circumduction is discussed in detail below.

4.2. Simulation results

4.2.1. Case I: Flexion-extension motion. Moving the real phalange in a flexion-extension motion is studied first. The flexion-extension motion is considered
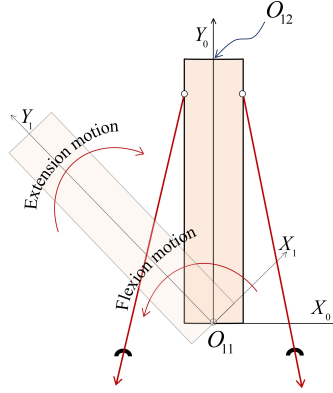
FIG. 5. Flexion-extension motion of the rea phalange about the Z_0-axis in radial view.

as the rotation of the phalange about the inertial Z_0-axis (joint axis in this case), as shown in Fig. 5.

Initially, the MTUs of the real phalange are subjected to a pre-tension of 0.005 N to attain a taut state. After that, the desired motion is imposed on the virtual phalange in flexion-extension motion by rotating it about the axis Z_0. The tip of the virtual phalange O_{12v} is commanded to move by an angle of $\frac{\pi^c}{6}$ counterclockwise, from its initial upright position ${}_0^0\bar{r}_{O_{12v}}$ as $\{0,\ 0.040,\ 0\}^T$ m, and then brought back to the initial posture following the trajectory profile. The desired trajectory polynomial for the motion of the tip of the virtual phalange is given by (25):

$$\dot{\theta}_d(t) = 0, \quad t \leq 10s;$$

$$\dot{\theta}_d(t) = 0.0001t^6 - 0.0048t^5 + 0.1155t^4 - 1.6127t^3 + 13.1947t^2$$
$$- 58.6431t + 109.4321, \quad 10s < t \leq 20s;$$

$$\dot{\theta}_d(t) = 0, \quad 20s < t \leq 40s;$$

$$\dot{\theta}_d(t) = 10^5(0.0015t^3 - 0.0396t^2 + 0.5864t - 3.7143), \quad 40s < t \leq 50s;$$

$$\dot{\theta}_d(t) = 0, \quad t > 50s.$$

(25)

This moves the phalange in flexion-extension motion in the inertial X_0-Y_0 plane. The rotation is permitted only about the Z_0-axis and the rotation about the other two mutually perpendicular axes X_0 and Y_0 constrained by the rotational couplings. Various joint properties considered for the phalange are given in Table 2.

The values of rotational stiffness K_{rx} and K_{ry} of 100 N·m/rad with matching damping to offer dynamic resistance to the movement are taken in the model to

TABLE 2. Joint properties of translational and rotational couplings.

Phalange	Direction	Translational stiffness [N/m] and damping [N·s/m]	Rotational stiffness [Nm/rad] and damping [N·m·s/rad]
Virtual and real phalange	X	$K_{tx} = 10^5$, $R_{tx} = 5$	$K_{rx} = 100$, $R_{rx} = 10$
	Y	$K_{ty} = 10^5$, $R_{ty} = 5$	$K_{ry} = 100$, $R_{ry} = 10$
	Z	$K_{tz} = 10^5$, $R_{tz} = 5$	$K_{rz} = 0$, $R_{rz} = 0$

provide constraints in the respective directions. This implies that the application of a moment of 10 N·m would cause an angular deformation of one-tenth of a radian at the joint. These rotational stiffnesses do not perfectly constrain the phalange but permit a very small angular motion about these axes on the basis, as mentioned above. Figure 6 shows the desired trajectory profile for the enforced motion based on Eq. (25). Figure 7 shows the posture of the virtual and real phalange during flexion-extension motion. Figure 8 shows the coordinates of the COM of the virtual and real phalanges over the time interval in the inertial frame. It is observed that the COM of the real phalange tracks the COM of the virtual phalange during the motion.
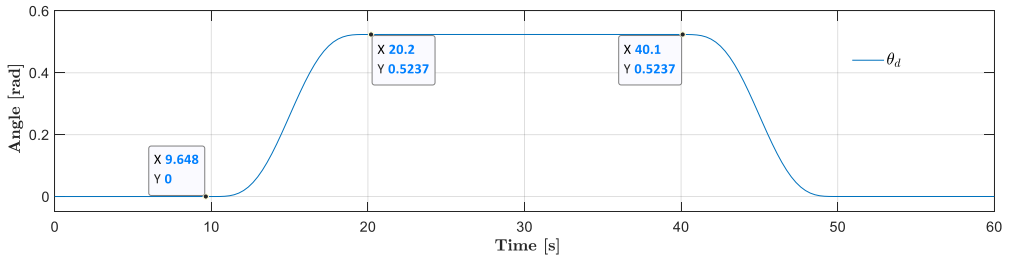
FIG. 6. Desired joint angle trajectory during flexion-extension motion about the Z_0-axis.
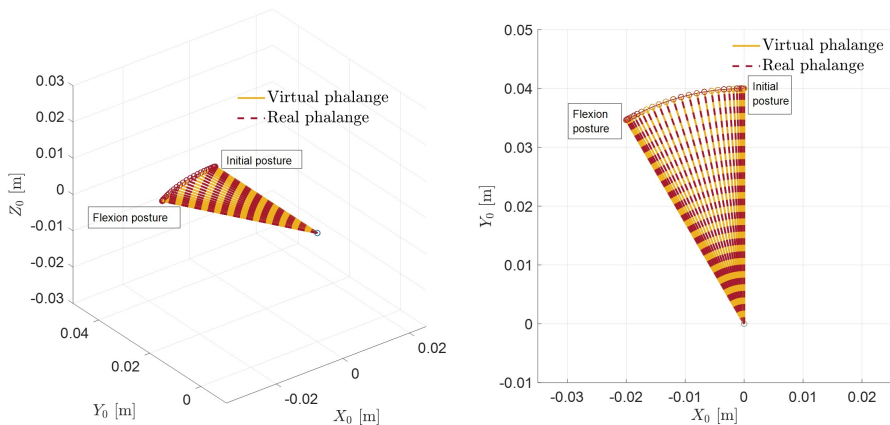
FIG. 7. Postures of the virtual and real phalanges during flexion-extension motion.
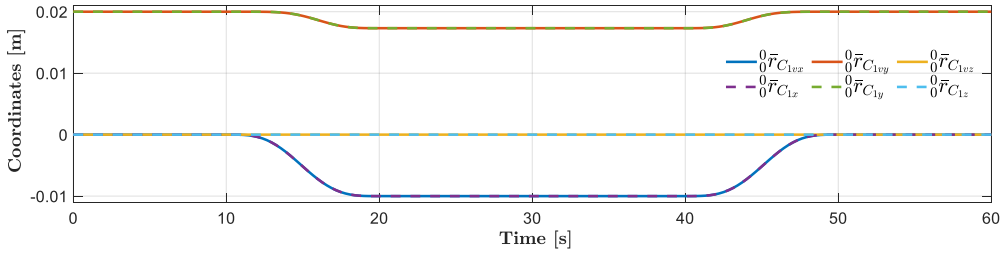
FIG. 8. Position of COM of virtual and real phalange during flexion-extension motion.

Based on the control strategy, the MTUs show a coordinated pattern of stretching out and relaxation. Figure 9 shows the variation of the controller force, extension patterns, and the forces generated corresponding to Hill's series-elastic elements (SE) of the MTUs. Figure 10 shows the pattern of the extensions and forces generated in Hill's PE elements of the MTUs. It is observed that the SE elements of the MTUs attain the equilibrium state under pre-tension quickly. While the PE elements of the MTUs take a longer time of about 6 s to attain the same, as these are strain-dependent non-linear elements with higher stiffness corresponding to higher strains.
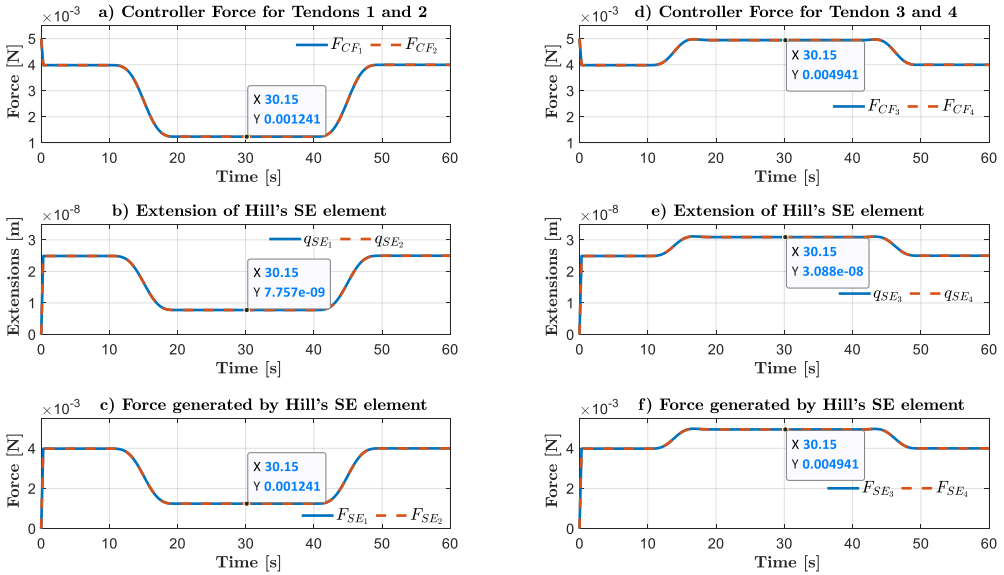
FIG. 9. MTC forces (a) and (d), extensions of Hill's SE elements (b) and (e), forces applied to the real phalange by muscle-tendon units through the Hill's SE elements (c) and (f) during flexion-extension motion.

During flexion motion, the extension patterns of q_{SE1}, q_{PE1} and q_{SE2}, q_{PE2} are such that they relax the MTU 1 and MTU 2, respectively, from the initial
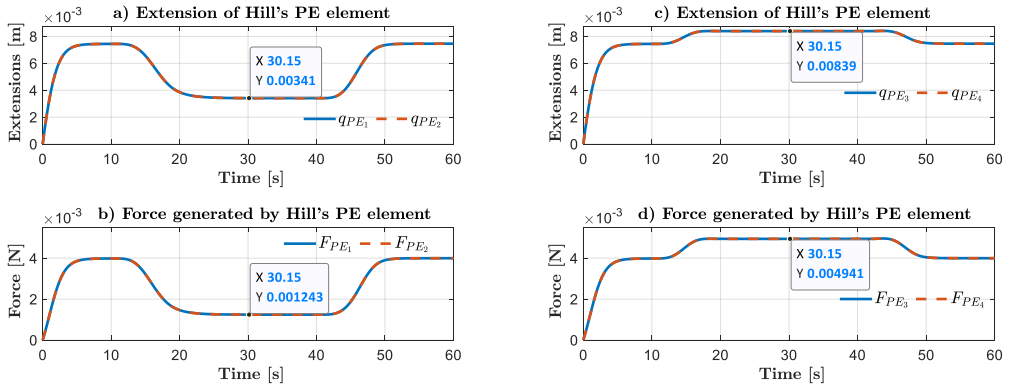
FIG. 10. Extensions of Hill's PE elements (a) and (c), forces generated by Hill's PE elements (b) and (d) during flexion-extension motion.

equilibrium state. Whereas the extension patterns of q_{SE3}, q_{PE3} and q_{SE4}, q_{PE4} are such that they extend the MTU 3 and MTU 4, respectively, beyond the initial equilibrium state. The resulting moments at the joint due to this pattern of extensions in the MTUs move the real phalange in flexion until the desired rotation angle is achieved in 10 s. After that, there is a dwell period of 20 s and the phalange remains in this state of equilibrium. Corresponding to this period, there is no change in the force in the MTUs, as shown in Figs. 9b, 9e and 10b, 10d, as there is no change in the extension patterns of the elements of the MTUs.

After that, the virtual phalange is commanded to move in the reverse direction, i.e., in extension to reach the initial posture in 10 s, as shown in the desired trajectory profile. It is observed here that during this part of the motion, the MTUs show a reversing of extension and force patterns to reach the initial posture, as expected. Following, it is desired to keep the phalange in this initial posture for 10 s to attain a steady state. There is no change in the extensions of the MTUs, and correspondingly there is no change in the momentum during the steady-state.

It is also observed in Figs. 9a, 9c and 9d, 9f that the muscle-tendon forces applied at the insertion locations on the real phalange track the controller forces imposed for the muscle activation by the MTCs. The excursion of the free ends of the MTUs can be obtained from the extension patterns of the PE elements of the MTUs in Fig. 10. The simulation results successfully demonstrate the control of the real phalange to achieve the flexion-extension motion as commanded by the virtual phalange, through the muscle-tendon actuation.

4.2.2. *Case II: Adduction-abduction motion.* In this motion, the phalange is rotated in adduction-abduction. The adduction-abduction is considered as the

rotation of the phalange about the X_0-axis (joint axis in this case), as shown in Fig. 11.
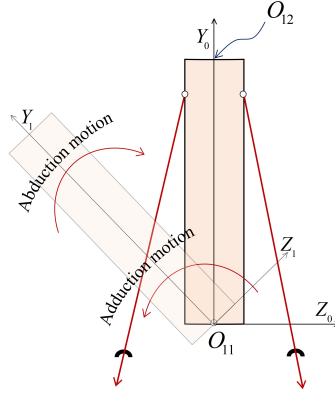

FIG. 11. Adduction-abduction motion of the real phalange about the X_0-axis in volar view.

The desired profile is applied to the virtual phalange for adduction-abduction motion. The tip of the virtual phalange O_{12v} is commanded to move by an angle of $\frac{\pi^c}{6}$ radians clockwise about the X_0-axis, from its initial upright position ${}^0_0\bar{r}_{O_{12v}}$ as $\{0,\ 0.040,\ 0\}^T$ m, and then brought back to its initial posture following the desired trajectory profile. This moves the phalange in adduction-abduction motion in the Y_0-Z_0 plane. The rotation is permitted only about the X_0-axis and the rotations about the other two mutually perpendicular Y_0- and Z_0-axes are constrained. The translational stiffness and damping coefficients are the same as those given in Table 2. The values of rotational joint stiffnesses K_{ry} and K_{rz} of 100 N·m/rad are taken in the model to provide constraints about the respective directions. This implies that the application of a moment of 10 N·m would cause an angular deformation of one-tenth of a radian at the joint. The corresponding matching rotational damping of couplings R_{ry} and R_{rz} is taken as 10 N·m·s/rad. The desired trajectory polynomial for the motion of the tip of the virtual phalange in adduction-abduction is given by (26):

$$\dot{\theta}_d(t) = 0, \quad t \leq 10s;$$

$$\dot{\theta}_d(t) = -0.0001t^6 + 0.0048t^5 - 0.1155t^4 + 1.6127t^3 - 13.1947t^2$$
$$+ 58.6431t - 109.4321, \quad 10s < t \leq 20s;$$

$$\dot{\theta}_d(t) = 0, \quad 20s < t \leq 40s; \tag{26}$$

$$\dot{\theta}_d(t) = 10^5(-0.0015t^3 + 0.0396t^2 - 0.5864t + 3.7143), \quad 40s < t \leq 50s;$$

$$\dot{\theta}_d(t) = 0, \quad t > 50s.$$

Figure 12 shows the desired trajectory profile for the adduction-abduction motion based on (26). Figure 13 shows the postures of the virtual and real phalanges during adduction-abduction motion. Figure 14 shows the coordinates of the COM of the virtual and real phalanges over the time interval $0 \leq t \leq 60$ s.
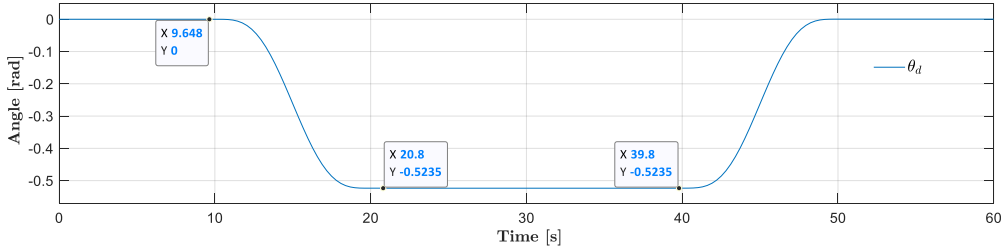

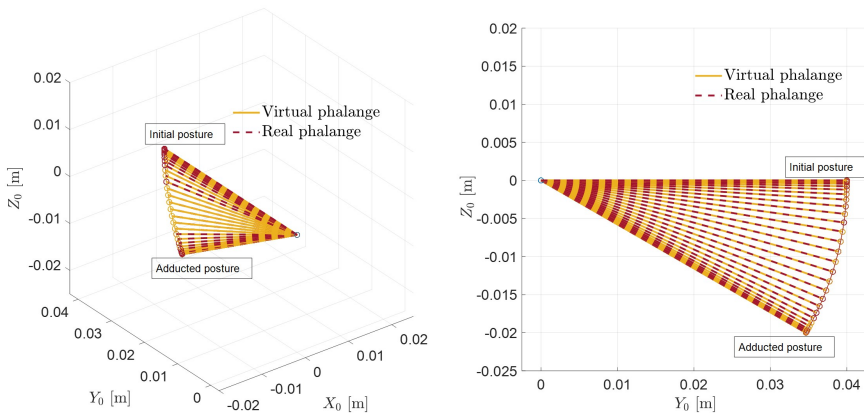FIG. 12. Desired joint angle trajectory during adduction-abduction motion about the X_0-axis.

FIG. 13. Postures of the virtual and real phalanges during adduction-abduction motion.
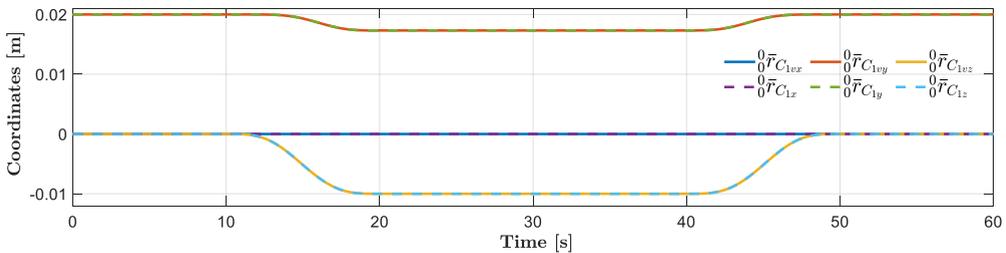
FIG. 14. Position of COM of virtual and real phalange during adduction-abduction motion.

Corresponding to the desired motion of the virtual phalange, the MTCs provide the necessary activation forces to the MTUs. Accordingly, the MTUs associated with the real phalange apply the corresponding forces at the tendon insertion locations to the desired motion. The extension patterns of q_{SE1}, q_{PE1} and q_{SE3}, q_{PE3} are such that they relax the MTU 1 and MTU 3, respectively,

from the equilibrium state during the adduction part of the motion. Whereas the extension patterns of q_{SE2}, q_{PE2} and q_{SE4}, q_{PE4} are such that they extend the MTU 2 and MTU 4, respectively. This pattern of extension in the MTUs generates a resulting moment about the joint axis of the real phalange to move it in adduction motion. After that, there is a dwell of 20 s, and then the phalange is commanded to rotate in the reverse direction for abduction motion. The extension and force patterns of the MTUs depict the reversal of motion.

Figures 15 and 16 show the variations of the extensions and forces generated by Hill's SE elements and PE elements of the MTUs, respectively.
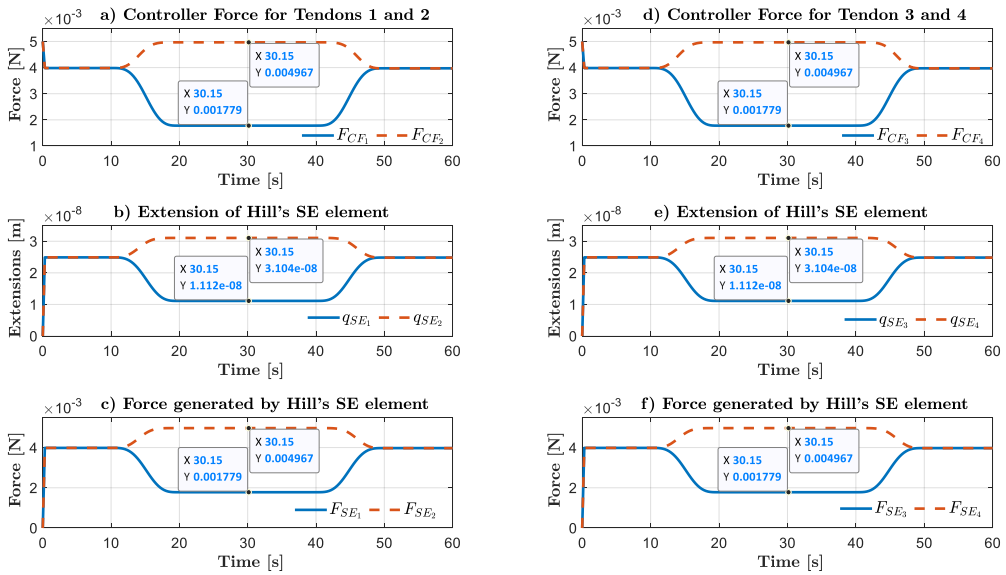
FIG. 15. MTC forces (a) and (d), extensions of Hill's SE elements (b) and (e), forces applied to the real phalange by MTUs through Hill's SE elements (c) and (f) during adduction-abduction motion.
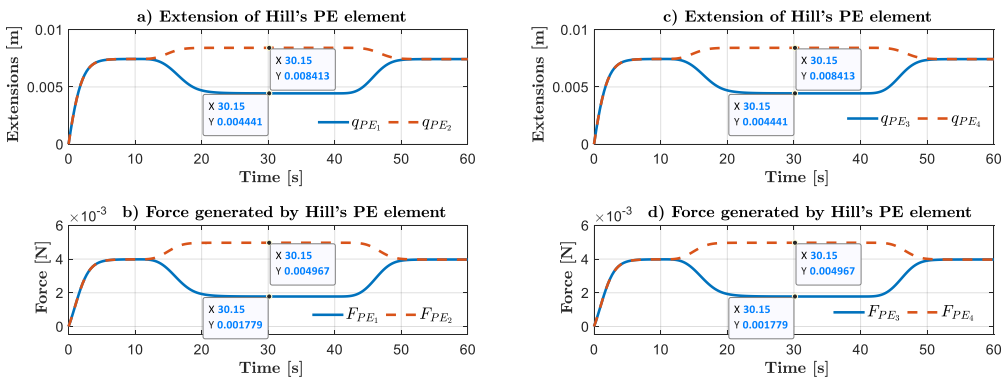

FIG. 16. Extensions of Hill's PE elements (a) and (c), forces generated by Hill's PE elements (b) and (d) during adduction-abduction motion.

4.2.3. Case III: Circumduction motion. Circumduction is a motion in which the phalange is rotated in a conical movement, as performed by a link in a ball and socket joint. This motion is modeled by considering a spherical type of joint connection at the phalange end. The phalange is relaxed to rotate about the X_0 and Z_0 axes while constraining the rotation about the Y_0-axis to prevent the rotation about the longitudinal axis of the phalange. The joint is held at its position by a translational coupling. The translational stiffness and damping coefficients are the same as those given in Table 2. The rotational stiffness K_{ry} is considered as 100 N·m/rad and rotational damping R_{ry} as 10 N·m·s/rad.

An initial pre-tension of 0.005 N is applied by the MTUs for maintaining the taut state for a period of 10 s. After that, the phalange is rotated in a conical pattern with a base radius of 10 mm in the inertial frame. Figure 17 shows the desired trajectory angle for the circumduction motion based on (27):

$$\overline{S}_{fd} = \overline{0}, \quad t \le 10s,$$

$$\overline{S}_{fd} = \left\{ -r\sin\theta_c\dot{\theta}_c \quad 0 \quad -r\cos\theta_c\dot{\theta}_c \right\}^T; \quad t > 10s, \tag{27}$$

where r is the base radius of the cone, θ_c is the rotation angle of the phalange, N is the angular speed of the desired motion in rpm (revolutions per minute), and $\dot{\theta}_c$ is the angular frequency of rotation given by (28):

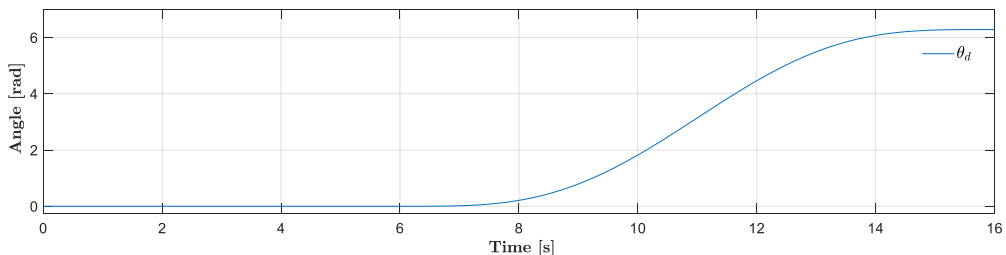$$\dot{\theta}_c = \frac{2\pi N}{60}. \tag{28}$$

Fig. 17. Desired joint angle trajectory during circumduction motion.

Figure 18 shows the posture of circumduction in three-dimensional space and in distal view, and Fig. 19 shows the position of the coordinates of the COM of the virtual and real phalange over time.

The MTUs show a variation in the pattern of muscle-tendon extensions as the position of the phalange changes with the motion in circumduction, as depicted in Figs. 20 and 21.

There is a coordinated pattern of extension and force generation among the muscle tendons. Accordingly, the forces are applied to the real phalange by different MTUs. The extension patterns of q_{SE1}, q_{SE3} and q_{PE1}, q_{PE3}, depicted in
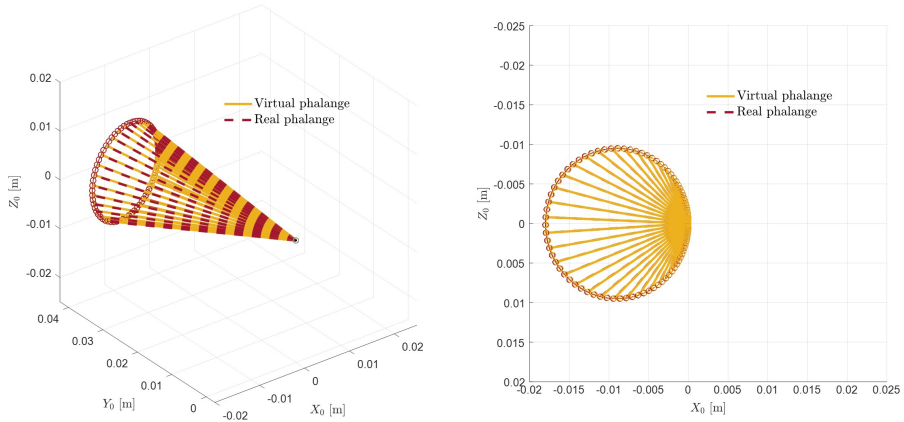
Fɪɢ. 18. Postures of the virtual and real phalanges during circumduction motion in three-dimensional space and in distal view.
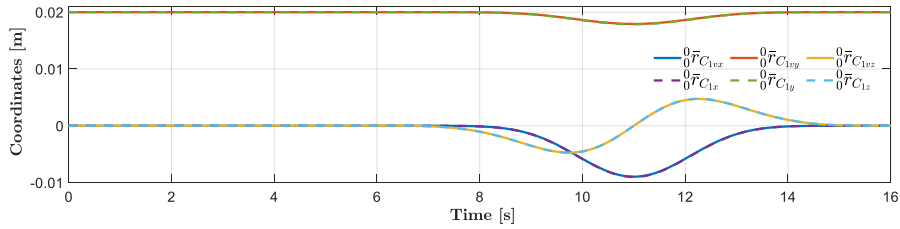

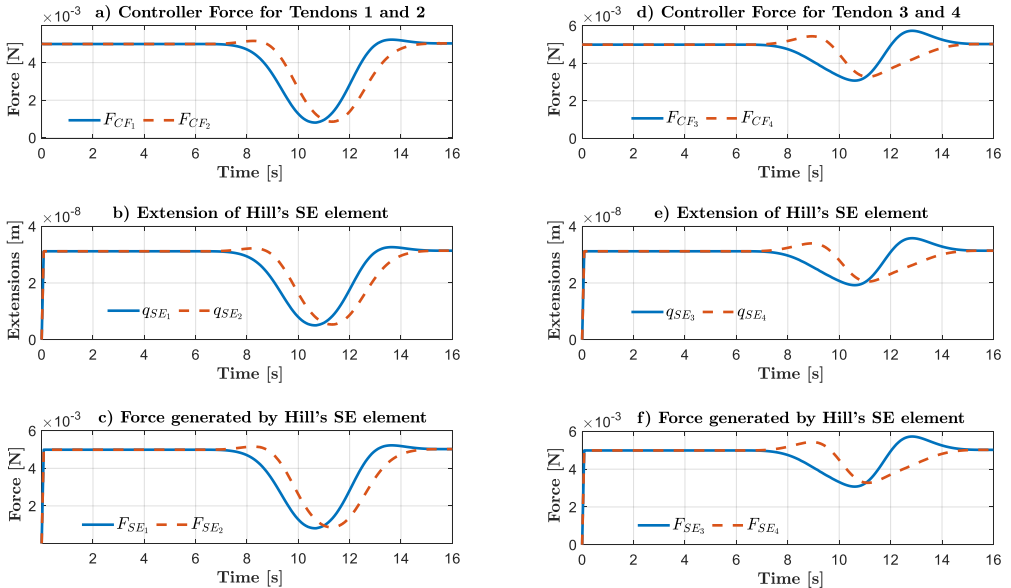Fɪɢ. 19. Position of COM of virtual and real phalange during circumduction motion.

Fɪɢ. 20. MTC forces (a) and (d), extensions of Hill's SE elements (b) and (e), forces applied to the real phalange by MTUs through Hill's SE elements (c) and (f) during circumduction motion.
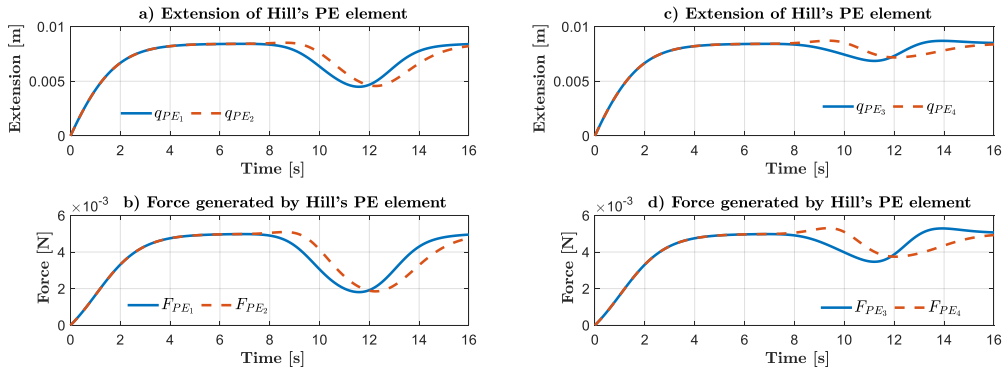
FIG. 21. Extensions of Hill's PE elements (a) and (c), forces generated by Hill's PE elements (b) and (d) during circumduction motion.

Figs. 20b, 20e and 21a, 21c, respectively, show the coordinated movement between the MTU 1 and 3. Similarly, there is coordinated movement between the MTU 2 and 4. This coordinated actuation of MTUs moves the real phalange in a pattern to track the conical path as commanded by the virtual phalange.

The simulation results successfully demonstrate the control of the real phalange to achieve the desired trajectory profiles through the muscle tendon.

5. CONCLUSION

A bond graph model for the musculoskeletal actuation of the phalange was developed systematically for the flexion-extension, adduction-abduction, and circumduction motion. The role of the CNS was emulated using the concept of a virtual phalange for the actuation of the real phalange through muscle tendons. The desired trajectory was imposed on the virtual phalange based on the intended motion. The inputs for the real phalange motion were taken from the virtual system. Pre-tension of muscle tendons is an essential requirement in the natural musculoskeletal system of the human body. It maintains the muscle-tendons in a taut condition. There is no transmission of force by the muscle tendons in the slackened state as they perform their function only under tension. The role of pre-tension was also incorporated in the developed muscle-tendon actuation system.

The real phalange tracks the desired virtual phalange trajectory by taking the input from the virtual MTCs in the form of muscle activation force. Based on this muscle activation force, corresponding extension patterns of the MTUs were developed. These extensions generated forces that were applied at the corresponding tendon insertion locations on the real phalange to bring the real phalange into motion. The MTUs were modeled as Hill's four-element muscle model. The model was simulated for flexion-extension, adduction-abduction, and circumduc-

tion motion, which are the common forms of motion for phalanges. Nevertheless, the described method can be applied to any limb motion in general.

So far, most of the research conducted on musculoskeletal behavior was on certain static postures and little was done to predict the dynamics of the system. In this work, predicting and analyzing the extensions and force patterns generated by the muscle-tendon structure considering dynamics was explored. To understand the dynamics of joint actuation through the muscle tendons, certain issues were needed to be addressed: the number of muscle tendons involved, the coordinated pattern of extensions among the associated muscle tendons, the force patterns to be applied by the MTUs, and the pre-tension. All these issues, which were required to be explored from the control point of view through the CNS, were addressed in this work.

References

1. J.N. Ingram, K.P. Körding, I.S. Howard, D.M. Wolpert, The statistics of natural hand movements, *Experimental Brain Research*, **188**(2): 223–236, 2008, doi: 10.1007/s00221-008-1355-3.

2. A. Freivalds, *Biomechanics of the Upper Limbs: Mechanics, Modeling and Musculoskeletal Injuries*, CRC Press, Boca Raton, 2011.

3. J.H.C. Wang, Q. Guo, B. Li, Tendon biomechanics and mechanobiology – A minireview of basic concepts and recent advancements, *Journal of Hand Therapy*, **25**(2): 133–141, 2012, doi: 10.1016/j.jht.2011.07.004.

4. T.J. Roberts, A.M. Gabaldón, Interpreting muscle function from EMG: Lessons learned from direct measurements of muscle force, *Integrative and Comparative Biology*, **48**(2): 312–320, 2008, doi: 10.1093/icb/icn056.

5. K.N. An, E.Y. Chao, W.P. Cooney, R.L. Linscheid, Forces in the normal and abnormal hand, *Journal of Orthopaedic Research*, **3**(2): 202–211, 1985, doi: 10.1002/jor.1100030210.

6. M.E. Johanson, F.J. Valero-Cuevas, V.R. Hentz, Activation patterns of the thumb muscles during stable and unstable pinch tasks, *Journal of Hand Surgery*, **26**(4): 698–705, 2001, doi: 10.1053/jhsu.2001.26188.

7. J.L. Sancho-Bru, A. Pérez-González, M. Vergara-Monedero, D. Giurintano, A 3-D dynamic model of human finger for studying free movements, *Journal of Biomechanics*, **34**(11): 1491–1500, 2001, doi: 10.1016/S0021-9290(01)00106-3.

8. L.A. Wojcik, Modeling of musculoskeletal structure and function using a modular bond graph approach, *Journal of Franklin Institute*, **340**(1): 63–76, 2003, doi: 10.1016/S0016-0032(03)00011-5.

9. F. Chen Chen, S. Appendino, A. Battezzato, A. Favetto, M. Mousavi, F. Pescarmona, Constraint study for a hand exoskeleton: Human hand kinematics and dynamics, *Journal of Robotics*, **2013**: 910961, 2013, doi: 10.1155/2013/910961.

10. A. Vaz, K. Singh, G. Dauphin-Tanguy, A Bond graph model for the actuation mechanism of musculo-skeletal joints, [in:] *Volume 2: Automotive Systems; Bioengineering and*

Biomedical Technology; Computational Mechanics; Controls; Dynamical Systems, pp. 69–75, 2008, doi: 10.1115/ESDA2008-59301.

11. A. Vaz, K. Singh, G. Dauphin-Tanguy, Bond graph model of extensor mechanism of finger based on hook-string mechanism, *Mechanism and Machine Theory*, **91**: 187–208, 2015, doi: 10.1016/j.mechmachtheory.2015.03.011.

12. N. Mishra, A. Vaz, Bond graph modeling of a 3-joint string-tube actuated finger prosthesis, *Mechanism and Machine Theory*, **117**: 1–20, 2017, doi: 10.1016/j.mechmachtheory.2017.06.018.

13. M. Santello, G. Baud-Bovy, H. Jörntell, Neural bases of hand synergies, *Frontiers in Computational Neuroscience*, **7**(23): 1–15, 2013, doi: 10.3389/fncom.2013.00023.

14. N. Mishra, A. Vaz, Development of trajectory and force controllers for 3-joint string-tube actuated finger prosthesis based on bond graph modeling, *Mechanism and Machine Theory*, **146**: 103719, 24 pages, 2020, doi: 10.1016/j.mechmachtheory.2019.103719.

15. R. Drake, A. Vogl, A. Mitchell, *Gray's Anatomy for Students*, 3rd Ed., Churchill Livingstone Elsevier, Canada, 2015.

16. Y.C. Fung, *Mechanical Properties of Living Tissues*, 2nd Ed., Springer, New York, 1993.

17. D. Karnopp, D. Margolis, R. Rosenberg, *System Dynamics*, 5th Ed., John Wiley & Sons, New Jersy, 2012.

18. B. Alexander, V. Kotiuk, Proportions of hand segments, *International Journal of Morphology*, **28**(3): 755–758, 2010.

19. H.E. Ash, A. Unsworth, Design of a surface replacement prosthesis for the proximal interphalangeal joint, *Proceedings of the Institution of Mechanical* Engineers, *Part H*: *Journal of Engineering in Medicine*, **214**(2): 151–163, 2000, doi: 10.1243/0954411001535327.

20. C.E. Garrido Varas, T.J.U. Thompson, Metric dimensions of the proximal phalanges of the human hand and their relationship to side, position, and asymmetry, *HOMO – Journal of Comparative Human Biology*, **62**(2): 126–143, 2011, doi: 10.1016/j.jchb.2010.07.005.

21. I.V. Grinyagin, E.V. Biryukova, M.A. Maier, Kinematic and dynamic synergies of human precision-grip movements, *Journal of Neurophysiology*, **94**(4): 2284–2294, 2005, doi: 10.1152/jn.01310.2004.

22. R. Arshad, *Modelling inhomogeneities within the human intervertebral disc*, Master Thesis, no. 04, Institute of Mechanics, Chair II, University of Stuttgart, 2004.

23. J. Yang, R. Chiou, A. Ruprecht, J. Vicario, L.A. Macphail, T.E. Rams, A new device for measuring density of jaw bones, *Dentomaxillofacial Radiology*, **31**: 313–316, 2002, doi: 10.1038/sj.dmfr.4600715.

24. J.H.C. Wang, Mechanobiology of tendon, *Journal of Biomechanics*, **39**(9): 1563–1582, 2006, doi: 10.1016/j.jbiomech.2005.05.011.

25. E.L. Secco, A. Visioli, G. Magenes, Minimum jerk motion planning for a prosthetic finger, *Journal of Robotic Systems*, **21**(7): 361–368, 2004, doi: 10.1002/rob.20018.